

1 **Sensitivity of Chemistry-Transport Model Simulations to the Duration of Chemical and**
2 **Transport Operators: A Case Study with GEOS-Chem v10-01**

3

4 S. Philip^{1,*}, R. V. Martin^{1,2} and C. A. Keller^{3,4}

5

6 ¹Department of Physics and Atmospheric Science, Dalhousie University, Halifax, Nova Scotia,
7 Canada

8 ²Harvard-Smithsonian Center for Astrophysics, Cambridge, Massachusetts, USA

9 ³School of Engineering and Applied Sciences, Harvard University, Cambridge, Massachusetts,
10 USA

11 ⁴Now at Universities Space Research Association / GESTAR, NASA GMAO Code 610.1,
12 Greenbelt, Maryland, USA

13

14 * Corresponding author: Sajeev Philip, Department of Physics and Atmospheric Science,
15 Dalhousie University, Halifax, NS, B3H 4R2, Canada (philip.sajeev@dal.ca)

16

17 **Abstract**

18 Chemistry-transport models involve considerable computational expense. Fine temporal
19 resolution offers accuracy at the expense of computation time. Assessment is needed of the
20 sensitivity of simulation accuracy to the duration of chemical and transport operators. We conduct
21 a series of simulations with the GEOS-Chem chemistry-transport model at different temporal and
22 spatial resolutions to examine the sensitivity of simulated atmospheric composition to operator
23 duration. Subsequently, we compare the species simulated with operator durations from 10 min to

24 60 min as typically used by global chemistry-transport models, and identify the operator durations
25 that optimize both computational expense and simulation accuracy. We find that longer continuous
26 transport operator duration increases concentrations of emitted species such as nitrogen oxides and
27 carbon monoxide since a more homogeneous distribution reduces loss through chemical reactions
28 and dry deposition. The increased concentrations of ozone precursors increase ozone production
29 with longer transport operator duration. Longer chemical operator duration decreases sulfate and
30 ammonium but increases nitrate due to feedbacks with in-cloud sulfur dioxide oxidation and
31 aerosol thermodynamics. The simulation duration decreases by up to a factor of 5 from fine (5
32 min) to coarse (60 min) operator duration. We assess the change in simulation accuracy with
33 resolution by comparing the root mean square difference in ground-level concentrations of
34 nitrogen oxides, secondary inorganic aerosols, ozone and carbon monoxide with a finer temporal
35 or spatial resolution taken as “truth”. Relative simulation error for these species increases by more
36 than a factor of 5 from the shortest (5 min) to longest (60 min) operator duration. Chemical operator
37 duration twice that of the transport operator duration offers more simulation accuracy per unit
38 computation. However, relative simulation error from coarser spatial resolution generally exceeds
39 that from longer operator duration; e.g. degrading from $2^\circ \times 2.5^\circ$ to $4^\circ \times 5^\circ$ increases error by an
40 order of magnitude. We recommend prioritizing fine spatial resolution before considering different
41 operator durations in offline chemistry-transport models. We encourage chemistry-transport model
42 users to specify in publications the durations of operators due to their effects on simulation
43 accuracy.

44 **1 Introduction**

45 Global and regional chemistry-transport models (CTMs) have a wide range of applications in
46 studies of climate, air quality, and biogeochemical cycling. The last few decades have witnessed

47 rapid development of modeling sophistication to tackle these issues, but that development is
48 associated with increasing computational expense. Typically, Eulerian models divide the
49 atmosphere into numerous (10^4 - 10^8) grid boxes and solve the mass continuity equation to simulate
50 atmospheric composition. Numerical solution of the mass continuity equation involves separating
51 the different chemical and transport processes (or operators) through operator splitting. The
52 concentrations of simulated species are sensitive to the duration of operators used in the CTM.
53 Attention is needed to understand how operator duration affects model performance.

54 Numerous studies have examined the sensitivity of simulations to grid resolution for ozone (Jang
55 et al., 1995; Esler et al., 2004; Ito et al., 2009; Yu et al., 2016), ozone production efficiency (Liang
56 and Jacobson 2000), and ozone sensitivity to precursor emissions (Cohan et al., 2006; Henderson
57 et al., 2010). Simulation error increases proportional to the size of the horizontal grid (Wild and
58 Prather, 2006; Prather et al., 2008). Biases can be reduced by simulating sub grid scale processes
59 such as emission plumes from point sources (Sillman et al., 1990; Valin et al., 2011), aircraft
60 exhaust (Kraabøl et al., 2002), ship exhaust (Vinken et al., 2011), mineral dust emissions (Ridley
61 et al., 2013), and lightning (Cooper et al., 2014). The spatial and temporal resolution of the
62 meteorological fields used in CTMs can also influence model processes (Bian et al., 2009). The
63 spatiotemporal variation of carbon monoxide is better represented with finer grid resolution (Wang
64 et al., 2004; Chen et al., 2009; Yan et al., 2014). Moreover, fine horizontal resolution is important
65 for air quality exposure assessment and health impact studies (Punger and West, 2013; Fountoukis
66 et al., 2013; Thompson et al., 2014; Li et al., 2015). Fine vertical resolution can better represent
67 the effects of convection (Rind et al., 2007; Arteta et al., 2009). Simulations are also sensitive to
68 operator durations (Mallet et al., 2007; Santillana et al., 2016), however, few studies have
69 examined this sensitivity.

70 CTMs solve the continuity equation for tens to hundreds of chemical species, each with number
71 density n , for individual grid boxes defined in the Eulerian model.

$$72 \quad \frac{\partial n}{\partial t} = -\nabla \cdot nU + P - L \quad (1)$$

73 $\partial n/\partial t$ represents the local temporal evolution of n . $-\nabla \cdot nU$ represents the transport flux divergence
74 term, where U is the wind velocity vector. P and L are the local production and loss terms
75 respectively. Typically, the above equation is discretized in space, and the continuity equation is
76 simulated as a system of coupled non-linear partial differential equations with chemical and
77 transport operators. These chemical and transport operators are usually simulated sequentially
78 through operator splitting to increase computational efficiency (Hundsdofer and Verwer, 2003).
79 The transport operator involves solving the 3-D advection equation using efficient numerical
80 schemes (Prather, 1986; Lin and Rood, 1996). Boundary layer mixing, convection, emission and
81 deposition are often simulated as individual operators. The chemical operator representing the
82 temporal evolution of local sources and sinks involves numerically solving a system of coupled
83 ordinary differential equations using efficient solvers (Jacobson and Turco, 1994; Damian et al.,
84 2002). The integration timestep in a differential equation solver is important for efficient and
85 accurate solution (Jacobson and Turco, 1994). Moreover, the model accuracy is affected by the
86 duration of chemical and transport operators (Mallet and Sportisse, 2006; Mallet et al., 2007), and
87 the order in which these operators are applied (Sportisse, 2000; Santillana et al., 2016). The
88 operator splitting method requires the coupling between individual operators to be negligible over
89 the operator duration. However, reducing operator durations increases computational expense.
90 Attention is needed to this tradeoff.

91 We examine the sensitivity of a CTM to operator duration by conducting a series of simulations at
92 different horizontal resolutions and operator durations. We then identify the optimal operator

93 duration from the range of operator durations from 10 min to 60 min usually used by global CTMs
94 (e.g., Horowitz et al., 2003; Huijnen et al. 2010). Section 2 describes the sensitivity simulations,
95 the method to quantify the simulation error, as well as the method to identify the simulation
96 operator durations that best account for both computational expense and simulation accuracy.
97 Comparison of the sensitivity simulations, description of resolution-dependent errors, and the
98 identification of appropriate chemical and transport operator durations are examined in section 3.

99 **2 Materials and Methods**

100 **2.1 GEOS-Chem simulations**

101 We conduct a series of sensitivity simulations with the GEOS-Chem CTM (version 10-01;
102 www.geos-chem.org) at different horizontal resolutions and operator durations to examine the
103 individual sensitivities to chemical and transport operator durations. The GEOS-Chem model (Bey
104 et al., 2001) is used by about 100 research groups worldwide to simulate the oxidant-aerosol
105 system. GEOS-Chem has the capability to be driven with several generations of assimilated
106 meteorological data from the Goddard Earth Observing System (GEOS) at the NASA Global
107 Modeling Assimilation Office (GMAO). For computational expedience, GEOS-Chem global
108 simulations are often conducted using horizontal resolutions of either $4^\circ \times 5^\circ$ or $2^\circ \times 2.5^\circ$ degraded
109 from the native resolution of GEOS meteorology. GEOS-Chem also has the capability for nested
110 regional simulations where the global model provides dynamic boundary condition to the finer
111 regional grids (Wang et al., 2004; Chen et al., 2009; Zhang et al., 2011; van Donkelaar et al., 2012).
112 We use the GEOS-5.2.0 meteorology available at a native horizontal resolution of $0.5^\circ \times 0.667^\circ$
113 (Rienecker et al., 2008). It includes three-hour averaged 2-D fields such as mixed layer depth, and
114 six-hour averaged 3-D fields such as zonal and meridional wind, and convective mass flux. The

115 height of the lowest level of the model is approximately 130 meters above the sea level, with 47
116 vertical levels.

117 GEOS-Chem performs species advection (A), vertical mixing (V), cloud convection (Z) and wet
118 deposition (W) for every transport operator duration (T), as well as dry deposition (D), emissions
119 (E), and chemistry (G) for every chemical operator duration (C) in the following order,

$$120 \qquad \qquad \qquad A(T) \cdot D(C) \cdot E(C) \cdot V(T) \cdot Z(T) \cdot G(C) \cdot W(T) \qquad \qquad (2)$$

121 The traditional transport operator durations are 30 minutes at 4° x 5° resolution, 15 minutes at 2°
122 x 2.5° resolution, and 10 min at 0.5° x 0.667° resolution. The traditional chemical operator duration
123 is set to either 60 min or twice the transport operator duration based on the Strang operator splitting
124 scheme (Strang, 1968) which follows T · C · T · T · C · T order repetitively with C = 2 × T.
125 Transport operations are repeated twice before a chemical operation when C = 2 × T. We also
126 consider an alternate splitting scheme which follows T · C · T · C order repetitively with C = T.
127 Changes in operator duration from C = 2 × T to C = T include effects of both time truncation (T ·
128 T to T) and operator splitting.

129 Advection is based on the multi-dimensional flux-form semi-Lagrangian advection scheme (Lin
130 and Rood, 1996; Lin et al., 1994), with an additional pressure-fixer algorithm implemented for the
131 conservation of species mass (Rotman et al., 2004). The cloud convection operator couples
132 transport by convection (Balkanski et al., 1993; Wu et al., 2007) with gas-aerosol wet deposition
133 (Liu et al., 2001; Wang et al., 2011; Amos et al., 2012). GEOS-Chem uses an internal integration
134 timestep of 5 min for convective mixing within the cloud convection operator. The wet deposition
135 operator includes scavenging by large-scale precipitation through first order operators, rainout and
136 washout (Balkanski et al., 1993). We use a non-local boundary layer mixing scheme for vertical

137 transport (Holtslag and Boville, 1993, Lin and McElroy, 2010). Emissions are processed through
138 the HEMCO module (Keller et al., 2014). A resistance-in-series method is used for dry deposition
139 of species (Wesely, 1989; Wang et al., 1998; Zhang et al., 2001; Fisher et al., 2011).

140 GEOS-Chem uses a Sparse Matrix Vectorized GEAR II chemistry solver (Jacobson and Turco,
141 1994; Jacobson, 1995; 1998). The oxidant-aerosol chemistry simulation includes organic and black
142 carbon (Park et al., 2003), mineral dust (Fairlie et al., 2007; Zender et al., 2003; Ginoux et al.,
143 2001), sea salt (Alexander et al., 2005; Jaegle et al., 2011), and the sulfate-nitrate-ammonium
144 system (Park et al., 2004). The photolysis frequency is calculated (Mao et al., 2010; Eastham et
145 al., 2014) at the middle of the chemical operator duration using the Fast-JX algorithm (Bian and
146 Prather, 2002). Simulation of gas-aerosol interactions are performed within the chemistry operator
147 by aerosol extinction effects on photolysis rates (Martin et al., 2003), and heterogeneous chemistry
148 (Jacob, 2000) including aerosol uptake of N_2O_5 (Evans and Jacob, 2005) and HO_2 (Mao et al.,
149 2013). The ISORROPIA II thermodynamic module (Fontoukis and Nenes, 2007) performs
150 aerosol-gas partitioning (Pye et al., 2009).

151 We conduct simulations for 2010 July at two horizontal resolutions of $4^\circ \times 5^\circ$ and $2^\circ \times 2.5^\circ$ globally,
152 and $0.5^\circ \times 0.667^\circ$ over the North America (140°W – 40°W , 10°N – 70°N) and East Asia (70°W –
153 150°W , 11°S – 55°N) nested regions. We use the $4^\circ \times 5^\circ$ global simulation to archive dynamic
154 boundary conditions every three hours for the nested simulations. We use one month spin up with
155 each GEOS-Chem simulation to reduce the influence of initial conditions.

156 **2.2 Computing platform**

157 We conduct all simulations on the same computing platform to compare their computational
158 performance. We use the Glooscap cluster of the Atlantic Computational Excellence Network

159 (ACENET) Consortium of Canadian Universities (<http://www.ace-net.ca/wiki/Glooscap>). The
160 operating system is Linux 4.8. We use Intel Fortran compiler version 12. Each GEOS-Chem
161 simulation is submitted as a 16-thread parallelized job on a single node.

162 We calculate the CPU time for the month of July for each operator separately using the Fortran-
163 intrinsic routine, CPU_TIME. We found this value identical to the one calculated using the Linux
164 command ‘qacct -j’. To reduce the effects of other jobs on the shared cluster, we repeat simulations
165 five times, while excluding data output operations to minimize sensitivity to system input/output,
166 and use the median to represent CPU time. We also report the standard error over the five
167 simulations.

168 **2.3 Assessing the relative simulation error**

169 We treat the simulation with the shortest operator duration as the most accurate. This approach
170 exploits the reduction in error associated with coupling across operators as operator duration
171 diminishes. Assessing simulation error versus operator duration through comparison with
172 observations is impaired by imperfect model processes, by the sparseness of measurements, and
173 by model-observation representativeness biases. We take as “truth” the concentrations simulated
174 with a chemical operator duration (C) of 10 minutes and a transport operator duration (T) of 5
175 minutes (represented as C10T05). Finer resolutions are computationally prohibitive. We define the
176 relative simulation error E_{sim}^s for species s as the root mean square error (RMSE) of the species
177 concentrations simulated with the finest resolution (“truth”) and the simulation under consideration
178 (Sim), normalized by the concentrations in simulation “truth”,

$$179 \quad E_{sim}^s = \frac{\sqrt{N} \sqrt{\sum_{i=1}^{i=N} (Truth_i^s - Sim_i^s)^2}}{\sum_{i=1}^{i=N} Truth_i^s} \quad (3)$$

180

181 where, i represents a particular grid box, with a total number of N grid boxes of interest. RMSE in
182 the numerator is chosen instead of absolute difference to more heavily penalize extrema.
183 Normalization with the mass of the “true” simulation is intended to cross-compare E_{sim}^s of different
184 species. E_{sim}^s captures the variation of a species s from the “true” simulation.

185 We focus on four key species relevant to atmospheric chemistry, namely nitrogen oxides ($\text{NO}_x =$
186 $\text{NO} + \text{NO}_2$), secondary inorganic aerosols (SIA: sum of sulfate, nitrate and ammonium), ozone
187 (O_3), and carbon monoxide (CO). These species represent a range of lifetimes from a day (NO_x)
188 to weeks (CO). The focus on SIA is designed to devote more attention to chemically active species
189 than to mineral dust and sea salt. We sample the instantaneous values of simulated ground-level
190 concentrations of these atmospheric species every 60 min to span the diurnal variation of chemical
191 environments. We focus on concentrations in July near the Earth’s surface when and where
192 chemical and transport timescales tend to be short.

193 **2.4 Identifying the optimal operator duration**

194 A practical way to select optimal chemical and transport operator durations is to identify the
195 simulation with the lowest error (E_{sim}^s) per unit of computation time. To quantify the simulation
196 accuracy per unit CPU time, we propose a simple metric, the CPU-time adjusted Composite
197 Normalized Error (CNE) which represents a tradeoff between the simulation accuracy, and the
198 associated computation expense. This is performed by normalizing the relative simulation error
199 E_{sim}^s for species s by the CPU time t for the simulation under consideration t_{sim} and for a reference
200 simulation t_{ref} , and taking the mean of the four species.

201

202

$$CNE = \left(\frac{1}{4} \times \sum_s \frac{E_{sim}^s}{E_{ref}^s} \right) \times \left(\frac{t_{sim}}{t_{ref}} \right) \quad (4)$$

203 We normalize E_{sim}^s by the reference E_{ref}^s so that the CPU-time adjusted Composite Normalized
 204 Error for each species is of similar magnitude. The variation of CNE across operator durations is
 205 unaffected by the choice of reference simulation; C10T10 used here. The relative value of CPU
 206 time versus simulation accuracy is subjective and depends on scientific objective. This definition
 207 of CNE gives equal weighting to the respective cost of CPU time and simulation accuracy. The
 208 simulation with the lowest CNE is used to identify an optimal chemical and transport operator
 209 duration.

210 **3 Results and discussion**

211 Figure 1 shows the computational performance for the series of GEOS-Chem simulations
 212 conducted here. The CPU time decreases by factors of 3-5 from fine to coarse operator duration.
 213 The CPU time increases by about a factor of 4 from $4^\circ \times 5^\circ$ to $2^\circ \times 2.5^\circ$ and another factor of 2 to a
 214 single nested simulation at $0.5^\circ \times 0.667^\circ$. The linearity from $4^\circ \times 5^\circ$ to $2^\circ \times 2.5^\circ$ implies that grid
 215 boxes are sufficiently large that CPU time is proportional to the number of grid boxes, and that
 216 transport integration timesteps constrained by the Courant-Freidrich-Lewy criterion (Courant et
 217 al., 1967) are largely unaffected by changes to grid box size at these resolutions. Comparison of
 218 individual CPU times for chemical and transport operators shows that performing a single cycle
 219 of all chemical operations takes ~ 4 times that of a single cycle of transport operations at the global
 220 scale. This factor is reduced for nested simulations due in part to the additional CPU time for
 221 simulating boundary conditions.

222 Figure 2 illustrates the sensitivity of the simulations to chemical and transport operators at $2^\circ \times$
 223 2.5° horizontal resolution. The left column shows the species concentrations for the “true”

224 simulation (C10T05). The middle column shows the difference in species concentrations from
225 doubling the transport operator duration. This doubling is in practice a change in time truncation
226 of the transport operator from $T \cdot C \cdot T \cdot T \cdot C \cdot T$ to $T \cdot C \cdot T \cdot C$ since the transport operator must
227 keep pace with the chemistry operator. Increasing the transport operator duration tends to increase
228 concentrations of emitted species like CO and NO_x over source regions since species are more
229 uniformly mixed by long continuous operator durations before loss processes such as dry
230 deposition and chemistry occur. More homogeneous fields have lower dry deposition rates as a
231 larger fraction is mixed aloft, and lower chemical loss rates depending on the chemical regime.
232 The increase in CO over source regions is partly associated with decreases in OH. Increasing
233 concentrations of ozone precursors increases ozone production (P[O₃]). Wild and Prather (2006)
234 similarly found that ozone production increases at coarser horizontal resolution. Increasing the
235 transport operator duration increases SIA components, especially over the source regions of East
236 Asia, North India, and North America.

237 The right column in Fig. 2 shows the change in species concentrations from increasing the
238 chemical operator duration. Hydroxyl radical concentrations increase, NO_x concentrations
239 decrease, and P[O₃] decreases with increasing chemical operator durations over source regions.
240 Berntsen and Isaken (1997) found that the error introduced by coarser chemical operator durations
241 is higher in polluted regions than the clean background due to the increased time lag, and invariant
242 production and loss across rapid chemical cycles. A longer chemical operator duration decreases
243 sulfate and ammonium but increases nitrate over source regions. Inspection of SO₂ and H₂O₂ fields
244 indicates that sulfate formation through H₂O₂ in clouds decreases at longer chemical operator
245 durations. In turn, SO₂ and NH₃ concentrations increase at longer chemical operator durations due
246 to the corresponding decreases in ammonium sulfate or ammonium bisulfate. The additional free

247 ammonia at longer chemical operator durations tends to promote regional ammonium nitrate
248 formation depending on local thermodynamics. An increase of total SIA mass with increasing
249 chemical operator duration is driven by nitrate and ammonium, and partially compensated by a
250 reduction in sulfate, especially downwind of source regions. We find similar spatial patterns for
251 other operator duration combinations, and other horizontal resolutions.

252 Figure 3 shows the sensitivity of simulated species to changes in operator duration (C20T10 to
253 C10T05) at two other horizontal resolutions (global $4^\circ \times 5^\circ$, and nested North America $0.5^\circ \times 0.67^\circ$
254 simulations) considered here. Spatial patterns of monthly mean ground-level concentrations, and
255 absolute differences are similar, albeit with finer spatial heterogeneity resolved in the nested
256 simulation. However, some resolution dependent differences do arise reflecting nonlinear
257 feedbacks.

258 Figures 4 shows the relative simulation error for nitrogen oxides, secondary inorganic aerosols,
259 ozone and carbon monoxide with varying operator durations at $2^\circ \times 2.5^\circ$ horizontal resolution.
260 Relative simulation errors for all these major species increase by more than a factor of 5 from the
261 shortest to longest operator duration. Errors increase fairly smoothly with increasing chemical and
262 transport operator duration until the transport operator duration exceeds 30 min. Then errors
263 increase by an order of magnitude for long lived species of O_3 and CO. The saw-tooth pattern for
264 CO versus O_3 reflects a greater sensitivity of CO to transport operator duration and a greater
265 sensitivity of O_3 to chemical operator duration. Relative simulation errors for other horizontal
266 resolutions follow similar pattern. These relative errors of 5% - 35% for NO_x and SIA are
267 comparable to typical model-observation errors of $\sim 30\%$ for NO_x (Boersma et al., 2008; Hudman
268 et al., 2006) and 20 - 40% for SIA (Philip et al., 2014; Heald et al., 2012). Operator duration errors

269 of <2% for O₃ and CO are smaller than typical model-observation errors of ~20% for ozone (Zhang
270 et al., 2011; Wang et al., 2009) and 10 - 20% for CO (Duncan et al., 2007; Shindell et al., 2006).

271 Figure 5 shows the difference in simulated species at 2° x 2.5° horizontal resolution for the GEOS-
272 Chem traditional (C30T15) minus the finest operator durations considered (C10T05). The spatial
273 variation for the monthly mean ground-level concentrations is generally within 5-15% for short
274 lived species like NO_x and SIA, and within 1% for longer lived species like O₃ and CO. Santillana
275 et al. (2016) similarly found an upper limit of 10% for operator splitting errors. However, the
276 maximum hourly spatial variation can exceed 50% for short lived species and 5% for longer lived
277 species. The spatial pattern of extrema resembles that of the monthly mean, albeit with more
278 heterogeneity from synoptic variation.

279 We also examined the diurnal variation and vertical profile of extrema. Extrema arise from all
280 times of day with a slight tendency for larger values for NO_x at night, for O₃ near sunrise and
281 sunset, and for SIA and CO near noon. Zonal mean vertical profiles exhibit largest differences in
282 the lower troposphere for NO_x and SIA, with more homogeneous differences throughout the
283 troposphere for O₃ and CO. Near the subtropical jets of the upper troposphere O₃ and CO have
284 maximum extrema of up to 3%.

285 Figure 6 shows the CPU-time adjusted Composite Normalized Error for the GEOS-Chem
286 simulations at various horizontal resolutions and operator durations. The CNE is significantly
287 higher with C = T than C = 2 x T. We confirmed this tendency with different choices of “truth”
288 (such as C05T05, C10T10) or reference (such as C10T05) simulations. This finding motivates the
289 traditional approach of using C = 2 x T in GEOS-Chem simulations. Applying the chemical
290 operator as frequently as the transport operator (with C = T) appears to increase computation cost

291 with little benefit in accuracy. The CNE for all three horizontal resolutions have noisy minima
292 with a chemical operator duration of 20 min and a transport operator duration of 10 min (C20T10).
293 A unit of computation time has a similar efficiency for a small range of operator durations from
294 10 min to 20 min. We found similar patterns in the variation of CNE with operator durations with
295 CNE calculated for selected domains, such as over Northern Hemisphere, nested model regions,
296 land grid boxes, and over the entire troposphere. We conducted additional simulations at $4^\circ \times 5^\circ$
297 horizontal resolution for January 2011 with a spin up of 7 months, and found similar patterns in
298 CNE.

299 The relative simulation error decreases by 40-50% (Fig. 4) by changing the operator duration from
300 the traditional (C30T15) to the optimal (C20T10) at $2^\circ \times 2.5^\circ$ horizontal resolution. The relative
301 spatial variations are $<20\%$ for NO_x and SIA, and $<1\%$ for O_3 and CO. However, the CPU time
302 increases by 20% by the decrease in operator duration.

303 Table 1 shows the relative simulation error at $4^\circ \times 5^\circ$ horizontal resolution with “truth” at $2^\circ \times 2.5^\circ$
304 resolution (C10T05) to investigate the tradeoff between horizontal resolution and operator
305 duration. The simulation error for all species at $4^\circ \times 5^\circ$ resolution increases by an order of
306 magnitude compared to $2^\circ \times 2.5^\circ$ resolution for any choice of operator duration tested here. The
307 error in this configuration is insensitive to operator duration, and dominated by representativeness
308 differences due to spatial structure resolved at $2^\circ \times 2.5^\circ$ resolution, but not at $4^\circ \times 5^\circ$ resolution.
309 Nonlinear chemistry at different horizontal resolutions (e.g., Wild and Prather, 2006) also plays a
310 role. Numerical errors due to advection processes generally exceed those from operator splitting
311 (e.g., Prather et al., 2008; Santillana et al., 2016). We therefore recommend prioritizing horizontal
312 resolution over operator duration for offline CTMs using time-averaged meteorological fields as
313 tested here. As meteorological fields used in CTMs become available at finer temporal and spatial

314 resolution, the value of shorter operator duration should further increase. We encourage CTM users
315 to specify in publication the duration of operators due to its effect on simulation accuracy.

316 **4 Conclusions**

317 The computational expense of chemistry-transport models warrants investigation into their
318 efficiency and accuracy. Solving the continuity equation in CTMs through operator splitting
319 method offers numerical efficiency, however, few studies have examined the implications of
320 operator duration on simulation accuracy. We conducted simulations with the GEOS-Chem model
321 for multiple choices of operator duration from 10 min to 60 min as typically used by global CTMs.
322 We found that longer continuous transport operator durations increase ozone precursors and ozone
323 production over source regions since a more homogeneous distribution reduces loss through
324 chemical reactions and dry deposition. Longer chemical operator durations decrease NO_x and
325 ozone production over source regions. Longer chemical operator durations reduce sulfate and
326 ammonium concentrations, however increase nitrate due to feedbacks with in-cloud SO₂ oxidation
327 and local aerosol thermodynamics.

328 We investigated the computational efficiency with the GEOS-Chem model, and found that the
329 simulation computation time decreases by up to a factor of 5 from short (C10T05) to long
330 (C60T60) operator duration. The chemical operator consumes about four times the CPU time of
331 the transport operator. We subsequently compared the root mean square differences in the ground-
332 level concentrations of nitrogen oxides, secondary inorganic aerosols (SIA), ozone and carbon
333 monoxide with a finer temporal or spatial resolution taken as “truth”, and estimated the relative
334 simulation error. The relative simulation error for these species increases by more than a factor of
335 5 from the shortest to longest operator duration. Monthly mean simulation errors of about 30% for

336 NO_x and SIA from long operator duration are comparable to typical model-observation errors,
337 while simulation errors for CO and O₃ tend to be less than 2% for operator duration < 30 min.

338 In order to account for simulation accuracy with computational cost, we proposed a metric, CPU-
339 time adjusted Composite Normalized Error that identifies the operator duration with respect to
340 CPU cost. We find greater efficiency of using $C = 2 \times T$ than $C = T$ for all horizontal resolutions.

341 The Composite Normalized Error exhibits a noisy minimum for a chemical operator duration of
342 20 min and transport operator duration of 10 min for the range of operator durations and horizontal
343 resolutions considered here. Nonetheless, the relative simulation error from changing horizontal
344 resolution exceeds that from changing operator durations within a horizontal resolution. We
345 recommend prioritizing fine spatial resolution before considering different operator durations in
346 offline CTMs with time-averaged archived meteorological fields as tested here. The importance
347 of shorter operator durations should increase with the availability of time-averaged meteorological
348 fields at higher temporal resolution. Short operator durations could offer even greater benefits to
349 simulation accuracy in online CTMs that offer meteorological fields at temporal resolutions closer
350 to operator duration. We encourage CTM users to specify in publications the durations of operators
351 due to their effects on simulation accuracy.

352

353

354

355

356

357 **Code Availability**

358 The GEOS-Chem code is freely accessible to the public, by following the guidelines in
359 <http://wiki.geos-chem.org/>). This work used GEOS-Chem version 10-01.

360

361 **Acknowledgements**

362 We thank Colette Heald, Daniel Jacob and Patrick Kim for useful comments at the early stages of
363 this research. We are grateful to three anonymous reviewers for helpful comments. This work was
364 supported by National Science and Engineering Research Council, Canada, and Atlantic
365 Computational Excellence Network (<http://www.ace-net.ca/>).

366

367 **References**

368 Alexander, B., Park, R. J., Jacob, D. J., Li, Q. B., Yantosca, R. M., Savarino, J., Lee, C. C. W.
369 and Thiemens, M. H.: Sulfate formation in sea-salt aerosols: Constraints from oxygen isotopes, *J.*
370 *Geophys. Res.*, 110, D10307, doi:10.1029/2004JD005659, 2005.

371
372 Amos, H. M., Jacob, D. J., Holmes, C. D., Fisher, J. A., Wang, Q., Yantosca, R. M., Corbitt, E.
373 S., Galarneau, E., Rutter, A. P., Gustin, M. S., Steffen, A., Schauer, J. J., Graydon, J. A., St
374 Louis, V. L., Talbot, R. W., Edgerton, E. S., Zhang, Y., and Sunderland, E. M.: Gas-particle
375 partitioning of atmospheric Hg(II) and its effect on global mercury deposition, *Atmos. Chem.*
376 *Phys.*, 12, 591-603, doi:10.5194/acp-12-591-2012, 2012.

377
378 Arteta, J., Marecal, V., and Riviere, E. D.: Regional modelling of tracer transport by tropical
379 convection – Part 2: Sensitivity to model resolutions, *Atmos. Chem. Phys.*, 9, 7101-7114,
380 doi:10.5194/acp-9-7101-2009, 2009.

381
382 Balkanski, Y. J., Jacob, D. J., Gardner, G. M., Graustein, W. C., and Turekian, K. K.: Transport
383 and residence times of tropospheric aerosols inferred from a global three-dimensional simulation
384 of ²¹⁰Pb, *J. Geophys. Res.*, 98, 20573-20586, doi:10.1029/93JD02456, 1993.

385

386

387

388 Berntsen, T. K., and Isaksen, I. S. A.: A global three-dimensional chemical transport model for
389 the troposphere: 1. Model description and CO and ozone results, *J. Geophys. Res.*, 102, 21239-
390 21280, doi:10.1029/97JD01140, 1997.

391

392 Bey, I., Jacob, D. J., Yantosca, R. M., Logan, J. A., Field, B. D., Fiore, A. M., Li, Q. B., Liu, H.
393 G. Y., Mickley, L. J., and Schultz, M. G.: Global modeling of tropospheric chemistry with
394 assimilated meteorology: Model description and evaluation, *J. Geophys. Res.*, 106, 23073-
395 23095, doi:10.1029/2001JD000807, 2001.

396

397 Bian, H., Chin, M., Rodriguez, J. M., Yu, H., Penner, J. E., and Strahan, S.: Sensitivity of aerosol
398 optical thickness and aerosol direct radiative effect to relative humidity, *Atmos. Chem. Phys.*, 9,
399 2375-2386, doi:10.5194/acp-9-2375-2009, 2009.

400

401 Bian, H., and Prather, M. J.: Fast-J2: Accurate simulation of stratospheric photolysis in global
402 chemical models, *J. Atmos. Chem.*, 41, 281-296, doi:10.1023/A:1014980619462, 2002.

403

404 Boersma, K. F., Jacob, D. J., Eskes, H. J., Pinder, R. W., Wang, J., and van der A, R. J.:
405 Intercomparison of SCIAMACHY and OMI tropospheric NO₂ columns: Observing the diurnal
406 evolution of chemistry and emissions from space, *J. Geophys. Res.*, 113, D16S26,
407 doi:10.1029/2007JD008816, 2008.

408

409 Chen, D., Wang, Y., McElroy, M. B., He, K., Yantosca, R. M., and Le Sager, P.: Regional CO
410 pollution and export in China simulated by the high-resolution nested-grid GEOS-Chem model,
411 *Atmos. Chem. Phys.*, 9, 3825-3839, 10.5194/acp-9-3825-2009, 2009.

412

413 Cohan, D. S., Hu, Y., and Russell, A. G.: Dependence of ozone sensitivity analysis on grid
414 resolution, *Atmos. Environ.*, 40, 126-135, doi:10.1016/j.atmosenv.2005.09.031, 2006.

415

416 Cooper, M., Martin, R. V., Wespes, C., Coheur, P., Clerbaux, C., and Murray, L. T.:
417 Tropospheric nitric acid columns from the IASI satellite instrument interpreted with a chemical
418 transport model: Implications for parameterizations of nitric oxide production by lightning, *J.*
419 *Geophys. Res.-Atmos.*, 119, 10068-10079, doi:10.1002/2014JD021907, 2014.

420

421 Courant, R., Friedrichs, K., and Lewy, H.: On partial difference equations of mathematical
422 physics, *IBM Journal of Research and Development*, 11, 215-234, doi:10.1147/rd.112.0215,
423 1967.

424

425 Damian, V., Sandu, M., Potra, G. R., and Carmichael: The kinetic preprocessor KPP-a software
426 environment for solving chemical kinetics, *Comput. Chem. Eng.*, 26, 1567-1579,
427 doi:10.1016/S0098-1354(02)00128-X, 2002.

428

429 Duncan, B. N., Logan, J. A., Bey, I., Megretskaya, I. A., Yantosca, R. M., Novelli, P. C., Jones,
430 N. B., and Rinsland, C. P.: Global budget of CO, 1988 –1997: Source estimates and validation
431 with a global model, *J. Geophys. Res.*, 112, D22301, doi:10.1029/2007JD008459, 2007.

432

433 Eastham, S. D., Weisenstein, D. K., and Barrett, S. R. H.: Development and evaluation of the
434 unified tropospheric–stratospheric chemistry extension (UCX) for the global chemistry-transport
435 model GEOS-Chem, *Atmos. Environ.*, 89, 52-63, doi:10.1016/j.atmosenv.2014.02.001, 2014.
436

437 Esler, J. G., Roelofs, G. J., Kohler, M. O., and O’Connor, F. M.: A quantitative analysis of grid-
438 related systematic errors in oxidising capacity and ozone production rates in chemistry transport
439 models, *Atmos. Chem. Phys.*, 4, 1781-1795, doi:10.5194/acp-4-1781-2004, 2004.
440

441 Evans, M. J., and Jacob, D. J.: Impact of new laboratory studies of N₂O₅ hydrolysis on global
442 model budgets of tropospheric nitrogen oxides, ozone, and OH, *Geophys. Res. Lett.*, 32, L09813,
443 doi:10.1029/2005GL022469, 2005.
444

445 Fairlie, T. D., Jacob, D. J., and Park, R. J.: The impact of transpacific transport of mineral dust in
446 the United States, *Atmos. Environ.*, 41, 1251-1266, doi:10.1016/j.atmosenv.2006.09.048, 2007.
447

448 Fisher, J. A., Jacob, D. J., Wang, Q., Bahreini, R., Carouge, C. C., Cubison, M. J., Dibb, J. E.,
449 Diehl, T., Jimenez, J. L., Leibensperger, E. M., Lu, Z., Meinders, M. B. J., Pye, H. O. T., Quinn,
450 P. K., Sharma, S., Streets, D. G., van Donkelaar, A., and Yantosca, R. M.: Sources, distribution,
451 and acidity of sulfate-ammonium aerosol in the Arctic in winter-spring, *Atmos. Environ.*, 45,
452 7301-7318, doi:10.1016/j.atmosenv.2011.08.030, 2011.
453

454 Fountoukis, C., Koraj, D., Denier van der Gon, H.A.C., Charalampidis, P. E., Pilinis, C., and
455 Pandis, S. N.: Impact of grid resolution on the predicted fine PM by a regional 3-D chemical
456 transport model, *Atmos. Environ.*, 68, 24-32, doi:10.1016/j.atmosenv.2012.11.008, 2013.
457

458 Fountoukis, C., and Nenes, A.: ISORROPIA II: a computationally efficient thermodynamic
459 equilibrium model for K⁺-Ca²⁺-Mg²⁺-NH₄⁺-Na⁺-SO₄²⁻-NO₃⁻-Cl⁻-H₂O aerosols, *Atmos. Chem.*
460 *Phys.*, 7, 4639-4659, doi:10.5194/acp-7-4639-2007, 2007.
461

462 Ginoux, P., Chin, M., Tegen, I., Prospero, J. M., Holben, B., Duboviki, O., and Lin, S. J.:
463 Sources and distributions of dust aerosols simulated with the GOCART model, *J. Geophys. Res.*,
464 106, 20255–20274, doi:10.1029/2000JD000053, 2001.
465

466 Heald, C. L., Collett Jr., J. L., Lee, T., Benedict, K. B., Schwandner, F. M., Li, Y., Clarisse, L.,
467 Hurtmans, D. R., Van Damme, M., Clerbaux, C., Coheur, P.-F., Philip, S., Martin, R. V., and
468 Pye, H. O. T.: Atmospheric ammonia and particulate inorganic nitrogen over the United States,
469 *Atmos. Chem. Phys.*, 12, 10295-10312, doi:10.5194/acp-12-10295-2012, 2012.
470

471 Henderson, B. H., Jeffries, H. E., Kim, B. U., and Vizuete, W. G.: The influence of model
472 resolution on ozone in industrial volatile organic compound plumes, *J. Air Waste Manage.*
473 *Assoc.*, 60, 1105–1117, doi:10.3155/1047-3289.60.9.1105, 2010.
474

475 Holtslag, A. A. M., and Boville, B. A.: Local Versus Nonlocal Boundary-Layer Diffusion in a
476 Global Climate Model, *J. Clim.*, 6, 1825-1842, doi:10.1175/1520-
477 0442(1993)006<1825:LVNBLD>2.0.CO;2, 1993.

478 Horowitz, L. W., Walters, S., Mauzerall, D. L., Emmons, L. K., Rasch, P. J., Granier, C., Tie, X.,
479 Lamarque, J., Schultz, M. G., Tyndall, G. S., Orlando, J. J., and Brasseur, G. P.: A global
480 simulation of tropospheric ozone and related tracers: Description and evaluation of MOZART,
481 version 2, *J. Geophys. Res.*, 108, 4784, doi:10.1029/2002JD002853, 2003.
482

483 Hudman, R. C.; Jacob, D. J., Turquety, S., Leibensperger, E. M., Murray, L. T., Wu, S., Gilliland,
484 A. B., Avery, M., Bertram, T. H., Brune, W., Cohen, R. C., Dibb, J. E., Flocke, F. M., Fried, A.,
485 Holloway, J., Neuman, J. A., Orville, R., Perring, A., Ren, X., Sachse, G. W., Singh, H. B.,
486 Swanson, A., and Wooldridge, P. J.: Surface and lightning sources of nitrogen oxides over the
487 United States: Magnitudes, chemical evolution, and outflow, *J. Geophys. Res.*, 112, D12S05,
488 doi:10.1029/2006JD007912, 2007.
489

490 Huijnen, V., Williams, J., van Weele, M., van Noije, T., Krol, M., Dentener, F., Segers, A.,
491 Houweling, S., Peters, W., de Laat, J., Boersma, F., Bergamaschi, P., van Velthoven, P., Le
492 Sager, P., Eskes, H., Alkemade, F., Scheele, R., Nédélec, P., and Pätz, H. -W.: The global
493 chemistry transport model TM5: description and evaluation of the tropospheric chemistry
494 version 3.0, *Geosci. Model Dev.*, 3, 445-473, doi:10.5194/gmd-3-445-2010, 2010.
495

496 Hundsdorfer, W., and Verwer, J.: Numerical solution of time-dependent advection-diffusion-
497 reaction equations, *Springer Series in Computational Mathematics*, 33, 325-417,
498 doi:10.1007/978-3-662-09017-6_4, 2003.
499

500 Ito, A., Sillman, S., and Penner J. E.: Global chemical transport model study of ozone response
501 to changes in chemical kinetics and biogenic volatile organic compounds emissions due to
502 increasing temperatures: Sensitivities to isoprene nitrate chemistry and grid resolution, *J.*
503 *Geophys. Res.*, 114, D09301, doi:10.1029/2008JD011254, 2009.
504

505 Jacob, D.: Heterogeneous chemistry and tropospheric ozone, *Atmos. Environ.*, 34, 2131-2159,
506 doi:10.1016/S1352-2310(99)00462-8, 2000.
507

508 Jacobson, M. Z.: Computation of global photochemistry with SMVGEAR II, *Atmos. Environ.*,
509 29, 2541-2546, doi:10.1016/1352-2310(95)00194-4, 1995.
510

511 Jacobson, M. Z.: Improvement of SMVGEAR II on vector and scalar machines through absolute
512 error tolerance control, *Atmos. Environ.*, 32, 791-796, doi:10.1016/S1352-2310(97)00315-4,
513 1998.
514

515 Jacobson, M., and Turco, R. P.: SMVGEAR - A SPARSE-MATRIX, VECTORIZED GEAR
516 CODE FOR ATMOSPHERIC MODELS, *Atmos. Environ.*, 28, 273-284, doi:10.1016/1352-
517 2310(94)90102-3, 1994.
518

519 Jaegle, L., Quinn, P. K., Bates, T. S., Alexander, B., and Lin, J.-T.: Global distribution of sea salt
520 aerosols: new constraints from in situ and remote sensing observations, *Atmos. Chem. Phys.*, 11,
521 3137-3157, doi:10.5194/acp-11-3137-2011, 2011.
522

523 Jang, J. C., Jeffries, H. E., and Tonnesen, S.: Sensitivity of ozone to model grid resolution - II.
524 Detailed process analysis for ozone chemistry, *Atmos. Environ.*, 29, 3101-3114,
525 doi:10.1016/1352-2310(95)00119-J, 1995.
526

527 Keller, C. A., Long, M. S., Yantosca, R. M., Da Silva, A. M., Pawson, S., and Jacob, D. J.:
528 HEMCO v1.0: a versatile, ESMF-compliant component for calculating emissions in atmospheric
529 models, *Geosci. Model Dev.*, 7, 1409-1417, doi:10.5194/gmd-7-1409-2014, 2014.
530

531 Kraabøl, A. G., Berntsen, T. K., Sundet, J. K., and Stordal, F.: Impacts of NO_x emissions from
532 subsonic aircraft in a global three-dimensional chemistry transport model including plume
533 processes, *J. Geophys. Res.*, 107, 4655, doi:10.1029/2001JD001019, 2002.
534

535 Li, Y., Henze, D. K., Jack, D., and Kinney, P.: The influence of air quality model resolution on
536 health impact assessment for fine particulate matter and its components, *Air Qual., Atmos.*
537 *Health*, 1-18, doi:10.1007/s11869-015-0321-z, 2015.
538

539 Liang, J., and Jacobson, M. Z.: Effects of subgrid segregation on ozone production efficiency in
540 a chemical model, *Atmos. Environ.*, 34, 2975-2982, doi:10.1016/S1352-2310(99)00520-8, 2000.
541

542 Lin, J., and McElroy, M. B.: Impacts of boundary layer mixing on pollutant vertical profiles in
543 the lower troposphere: Implications to satellite remote sensing, *Atmos. Environ.*, 44, 1726-1739,
544 doi:10.1016/j.atmosenv.2010.02.009, 2010.
545

546 Lin, S., and Rood, R. B.: Multidimensional Flux-Form Semi-Lagrangian Transport Schemes,
547 *Mon. Weather Rev.*, 124, 2046-2070, doi:10.1175/1520-
548 0493(1996)124<2046:MFFSLT>2.0.CO;2, 1996.
549

550 Lin, S., Chao, W. C., Sud, Y. C., and Walker, G. K.: A Class of the van Leer-type Transport
551 Schemes and Its Application to the Moisture Transport in a General Circulation Model, *Mon.*
552 *Weather Rev.*, 122, 1575-1593, doi:10.1175/1520-0493(1994)122<1575:ACOTVL>2.0.CO;2,
553 1994.
554

555 Liu, H. Y., Jacob, D. J., Bey, I., and Yantosca, R. M.: Constraints from Pb-210 and Be-7 on wet
556 deposition and transport in a global three-dimensional chemical tracer model driven by
557 assimilated meteorological fields, *J. Geophys. Res.*, 106, 12109-12128,
558 doi:10.1029/2000JD900839, 2001.
559

560 Mallet, V. and Sportisse, B.: Uncertainty in a chemistry-transport model due to physical
561 parameterizations and numerical approximations: An ensemble approach applied to ozone
562 modeling, *J. Geophys. Res.*, 111, D01302, doi:10.1029/2005JD006149, 2006.
563

564 Mallet, V., Pourchet, A., Quélo, D., and Sportisse, B.: Investigation of some numerical issues in
565 a chemistry-transport model: Gas-phase simulations, *J. Geophys. Res.*, 112, D15301,
566 doi:10.1029/2006JD008373, 2007.
567

568 Mao, J., Jacob, D. J., Evans, M. J., Olson, J. R., Ren, X., Brune, W. H., St Clair, J. M., Crouse,
569 J. D., Spencer, K. M., Beaver, M. R., Wennberg, P. O., Cubison, M. J., Jimenez, J. L., Fried, A.,
570 Weibring, P., Walega, J. G., Hall, S. R., Weinheimer, A. J., Cohen, R. C., Chen, G., Crawford, J.
571 H., McNaughton, C., Clarke, A. D., Jaegle, L., Fisher, J. A., Yantosca, R. M., Le Sager, P., and
572 Carouge, C.: Chemistry of hydrogen oxide radicals (HO_x) in the Arctic troposphere in spring,
573 *Atmos. Chem. Phys.*, 10, 5823-5838, doi:10.5194/acp-10-5823-2010, 2010.
574
575 Mao, J., Fan, S., Jacob, D. J., and Travis, K. R.: Radical loss in the atmosphere from Cu-Fe
576 redox coupling in aerosols, *Atmos. Chem. Phys.*, 13, 509-519, doi:10.5194/acp-13-509-2013,
577 2013.
578
579 Martin, R. V., Jacob, D. J., Yantosca, R. M., Chin, M., and Ginoux, P.: Global and regional
580 decreases in tropospheric oxidants from photochemical effects of aerosols, *J. Geophys. Res.*,
581 108, 4097, doi:10.1029/2002JD002622, 2003.
582
583 Park, R. J., Jacob, D. J., Chin, M., and Martin, R. V.: Sources of carbonaceous aerosols over the
584 United States and implications for natural visibility, *J. Geophys. Res.-Atmos.*, 108, 4355,
585 doi:10.1029/2002JD003190, 2003.
586
587 Park, R. J., Jacob, D. J., Field, B. D., Yantosca, R. M., and Chin, M.: Natural and transboundary
588 pollution influences on sulfate-nitrate-ammonium aerosols in the United States: Implications for
589 policy, *J. Geophys. Res.-Atmos.*, 109, D15204, doi:10.1029/2003JD004473, 2004.
590
591 Philip, S., Martin, R. V., van Donkelaar, A., Lo, J. W.-H., Wang, Y., Chen, D., Zhang, L.,
592 Kasibhatla, P. S., Wang, S. W., Zhang, Q., Lu, Z., Streets, D. G., Bittman, S., and Macdonald, D.
593 J.: Global chemical composition of ambient fine particulate matter for exposure assessment,
594 *Environ. Sci. Technol.*, 48, 13060-13068, doi:10.1021/es502965b, 2014.
595
596 Prather, M. J.: Numerical advection by conservation of second-order moments, *J. Geophys. Res.*,
597 91, 6671-6681, doi:10.1029/JD091iD06p06671, 1986.
598
599 Prather, M. J., Zhu, X., Strahan, S. E., Steenrod, S. D., and Rodriguez, J. M.: Quantifying errors
600 in trace species transport modeling, *Proc. Natl. Acad. Sci. U. S. A.*, 105, 19617-19621,
601 doi:10.1073/pnas.0806541106, 2008.
602
603 Pungler, E. M., and West, J. J.: The effect of grid resolution on estimates of the burden of ozone
604 and fine particulate matter on premature mortality in the USA, *Air Qual., Atmos. Health*, 6, 563-
605 573, doi:10.1007/s11869-013-0197-8, 2013.
606
607 Pye, H. O. T., Liao, H., Wu, S., Mickley, L. J., Jacob, D. J., Henze, D. K., and Seinfeld, J. H.:
608 Effect of changes in climate and emissions on future sulfate-nitrate-ammonium aerosol levels in
609 the United States, *J. Geophys. Res.*, 114, D01205, doi:10.1029/2008JD010701, 2009.
610
611
612

613 Rienecker, M. M., Suarez, M. J., Todling, R., Bacmeister, J., Takacs, L., Liu, H.-C., Gu, W.,
614 Sienkiewicz, M., Koster, R. D., Gelaro, R., Stajner, I., and Nielsen, J. E.: The GEOS-5 Data
615 Assimilation System-Documentation of versions 5.0.1 and 5.1.0, and 5.2.0. NASA Tech. Rep.
616 Series on Global Modeling and Data Assimilation, NASA/TM-2008-104606, vol. 27, Goddard
617 Space Flight Center, Greenbelt, Maryland, USA, 92 p., 2008.
618

619 Ridley, D. A., Heald, C. L., Pierce, J. R., and Evans, M. J.: Toward resolution-independent dust
620 emissions in global models: Impacts on the seasonal and spatial distribution of dust, *Geophys.*
621 *Res. Lett.*, 40, 2873–2877, doi:10.1002/grl.50409, 2013.
622

623 Rind, D., Lerner, J., Jonas, J., and McLinden, C.: Effects of resolution and model physics on
624 tracer transports in the NASA Goddard Institute for Space Studies general circulation models, *J.*
625 *Geophys. Res.*, 112, D09315, doi:10.1029/2006JD007476, 2007.
626

627 Rotman, D. A., Atherton, C. S., Bergmann, D. J., Cameron-Smith, P. J., Chuang, C. C., Connel,
628 P. S., Dignon, J. E., Franz, A., Grant, K. E., Kinnison, D. E., Molenkamp, C. R., Proctor, D. D.,
629 and Tannahill, J. R.: IMPACT, the LLNL 3-D global atmospheric chemical transport model for
630 the combined troposphere and stratosphere: Model description and analysis of ozone and other
631 trace gases, *J. Geophys. Res.*, 109, D04303, doi:10.1029/2002JD003155, 2004.
632

633 Santillana, M., Zhang, L., and Yantosca, R.: Estimating numerical errors due to operator splitting
634 in global atmospheric chemistry models: Transport and chemistry, *J. Comput. Phys.*, 305, 372-
635 386, doi:10.1016/j.jcp.2015.10.052, 2016.
636

637 Shindell, D. T., Faluvegi, G., Stevenson, D. S., Krol, M. C., Emmons, L. K., Lamarque, J.-F.,
638 Petron, G., Dentener, F. J., Ellingsen, K., Schultz, M. G., Wild, O., Amann, M., Atherton, C. S.,
639 Bergmann, D. J., Bey, I., Butler, T., Cofala, J., Collins, W. J., Derwent, R. G., Doherty, R. M.,
640 Drevet, J., Eskes, H. J., Fiore, A. M., Gauss, M., Hauglustaine, D. A., Horowitz, L. W., Isaksen,
641 I. S. A., Lawrence, M. G., Montanaro, V., Muller, J. F., Pitari, G., Prather, M. J., Pyle, J. A.,
642 Rast, S., Rodriguez, J. M., Sanderson, M. G., Savage, N. H., Strahan, S. E., Sudo, K., Szopa, S.,
643 Unger, N., van Noije, T. P. C., and Zeng, G.: Multimodel simulations of carbon monoxide:
644 Comparison with observations and projected near-future changes, *J. Geophys. Res.*, 111,
645 D19306, doi:10.1029/2006JD007100, 2006.
646

647 Sillman, S., Logan, J. A., and Wofsy, S. C.: A regional scale model for ozone in the United
648 States with subgrid representation of urban and power plant plumes, *J. Geophys. Res.*, 95, 5731-
649 5748, doi:10.1029/JD095iD05p05731, 1990.
650

651 Sportisse, B.: An analysis of operator splitting techniques in the stiff case, *J. Comput. Phys.*, 161,
652 140-168, doi:10.1006/jcph.2000.6495, 2000.
653

654 Strang, G.: On the construction and comparison of difference schemes, *SIAM J. Numer. Anal.*, 5,
655 506-517, doi:10.1137/0705041, 1968.
656
657

658 Thompson, T. M., Saari, R. K., and Selin, N. E.: Air quality resolution for health impact
659 assessment: influence of regional characteristics, *Atmos. Chem. Phys.*, 14, 969-978,
660 doi:10.5194/acp-14-969-2014, 2014.

661
662 van Donkelaar, A., Zhang, L., Chen, D., Martin, R. V., Pasch, A. N., Szykman, J. J., and Wang,
663 Y. X.: Improving the accuracy of daily satellite-derived ground-level fine aerosol concentration
664 estimates for North America, *Environ. Sci. Technol.*, 46, 11971-11978, doi:10.1021/es3025319,
665 2012.

666
667 Valin, L. C., Russell, A. R., Hudman, R. C., and Cohen, R. C.: Effects of model resolution on the
668 interpretation of satellite NO₂ observations, *Atmos. Chem. Phys.*, 11, 11647-11655,
669 doi:10.5194/acp-11-11647-2011, 2011.

670
671 Vinken, G. C. M., Boersma, K. F., Jacob, D. J., and Meijer, E. W.: Accounting for non-linear
672 chemistry of ship plumes in the GEOS-Chem global chemistry transport model, *Atmos. Chem.*
673 *Phys.*, 11, 11707-11722, doi:10.5194/acp-11-11707-2011, 2011.

674
675 Wang, Q., Jacob, D. J., Fisher, J. A., Mao, J., Leibensperger, E. M., Carouge, C. C., Le Sager, P.,
676 Kondo, Y., Jimenez, J. L., Cubison, M. J., and Doherty, S. J.: Sources of carbonaceous aerosols
677 and deposited black carbon in the Arctic in winter-spring: implications for radiative forcing,
678 *Atmos. Chem. Phys.*, 11, 12453-12473, doi:10.5194/acp-11-12453-2011, 2011.

679
680 Wang, H., Jacob, D. J., Le Sager, P., Streets, D. G., Park, R. J., Gilliland, A. B., and van
681 Donkelaar, A.: Surface ozone background in the United States: Canadian and Mexican pollution
682 influences, *Atmos. Environ.*, 43, 1310-1319, doi:10.1016/j.atmosenv.2008.11.036, 2009.

683
684 Wang, Y., Jacob, D. J., and Logan, J. A.: Global simulation of tropospheric O₃-NO_x-hydrocarbon
685 chemistry: 1. Model formulation, *J. Geophys. Res.*, 103, 10713-10725, doi:10.1029/98JD00158,
686 1998.

687
688 Wang, Y. X., McElroy, M. B., Jacob D. J., and Yantosca, R. M.: A nested grid formulation for
689 chemical transport over Asia: Applications to CO, *J. Geophys. Res.*, 109,
690 doi:10.1029/2004JD005237, 2004.

691
692 Wesely, M. L.: Parameterization of surface resistances to gaseous dry deposition in regional-
693 scale numerical models, *Atmos. Environ.*, 23, 1293-1304, doi:10.1016/0004-6981(89)90153-4,
694 1989.

695
696 Wild, O., and Prather, M. J.: Global tropospheric ozone modeling: Quantifying errors due to grid
697 resolution, *J. Geophys. Res.*, 111, D11305, doi:10.1029/2005JD006605, 2006.

698
699 Wu, S., Mickley, L. J., Jacob, D. J., Logan, J. A., Yantosca, R. M. and Rind, D.: Why are there
700 large differences between models in global budgets of tropospheric ozone?, *J. Geophys. Res.*,
701 112, D05302, doi:10.1029/2006JD007801, 2007.

702

703 Yan, Y.-Y., Lin, J.-T., Kuang, Y., Yang, D., and Zhang, L.: Tropospheric carbon monoxide over
704 the Pacific during HIPPO: two-way coupled simulation of GEOS-Chem and its multiple nested
705 models, *Atmos. Chem. Phys.*, 14, 12649-12663, doi:10.5194/acp-14-12649-2014, 2014.
706
707 Yu, K., Jacob, D. J., Fisher, J. A., Kim, P. S., Marais, E. A., Miller, C. C., Travis, K. R., Zhu, L.,
708 Yantosca, R. M., Sulprizio, M. P., Cohen, R. C., Dibb, J. E., Fried, A., Mikoviny, T., Ryerson, T.
709 B., Wennberg, P. O., and Wisthaler, A.: Sensitivity to grid resolution in the ability of a chemical
710 transport model to simulate observed oxidant chemistry under high-isoprene conditions, *Atmos.*
711 *Chem. Phys. Discuss.*, doi:10.5194/acp-2015-980, in review, 2016.
712
713 Zender, C. S., Bian, H., and Newman, D.: The mineral dust entrainment and deposition (DEAD)
714 model: description and 1990s dust climatology, *J. Geophys. Res.*, 108, 4416,
715 doi:10.1029/2002JD002775, 2003.
716
717 Zhang, L. M., Gong, S. L., Padro, J. and Barrie, L.: A size-segregated particle dry deposition
718 scheme for an atmospheric aerosol module, *Atmos. Environ.*, 35, 549-560, doi:10.1016/S1352-
719 2310(00)00326-5, 2001.
720
721 Zhang, L., Jacob, D. J., Downey, N. V., Wood, D. A., Blewitt, D., Carouge, C. C., van
722 Donkelaar, A., Jones, D. B. A., Murray, L. T., and Wang, Y.: Improved estimate of the policy-
723 relevant background ozone in the United States using the GEOS-Chem global model with $1/2^\circ \times$
724 $2/3^\circ$ horizontal resolution over North America, *Atmos. Environ.*, 45, 6769-6776,
725 doi:10.1016/j.atmosenv.2011.07.054, 2011.
726
727
728
729
730
731
732
733
734
735
736
737
738
739
740
741
742
743
744
745
746

747 Table 1: Comparison of mean* relative simulation error versus horizontal resolution, with “truth”
748 defined at 2° x 2.5° horizontal resolution

749

Species	Mean relative simulation error (unitless)	
	4° x 5° resolution	2° x 2.5° resolution
Nitrogen oxides	2.1	0.092
Secondary inorganic aerosols	1.0	0.14
Ozone	0.17	0.004
Carbon monoxide	0.36	0.005

750

751 * Mean taken for operator durations ≤ 30 min.

752

753

754

755

756

757

758

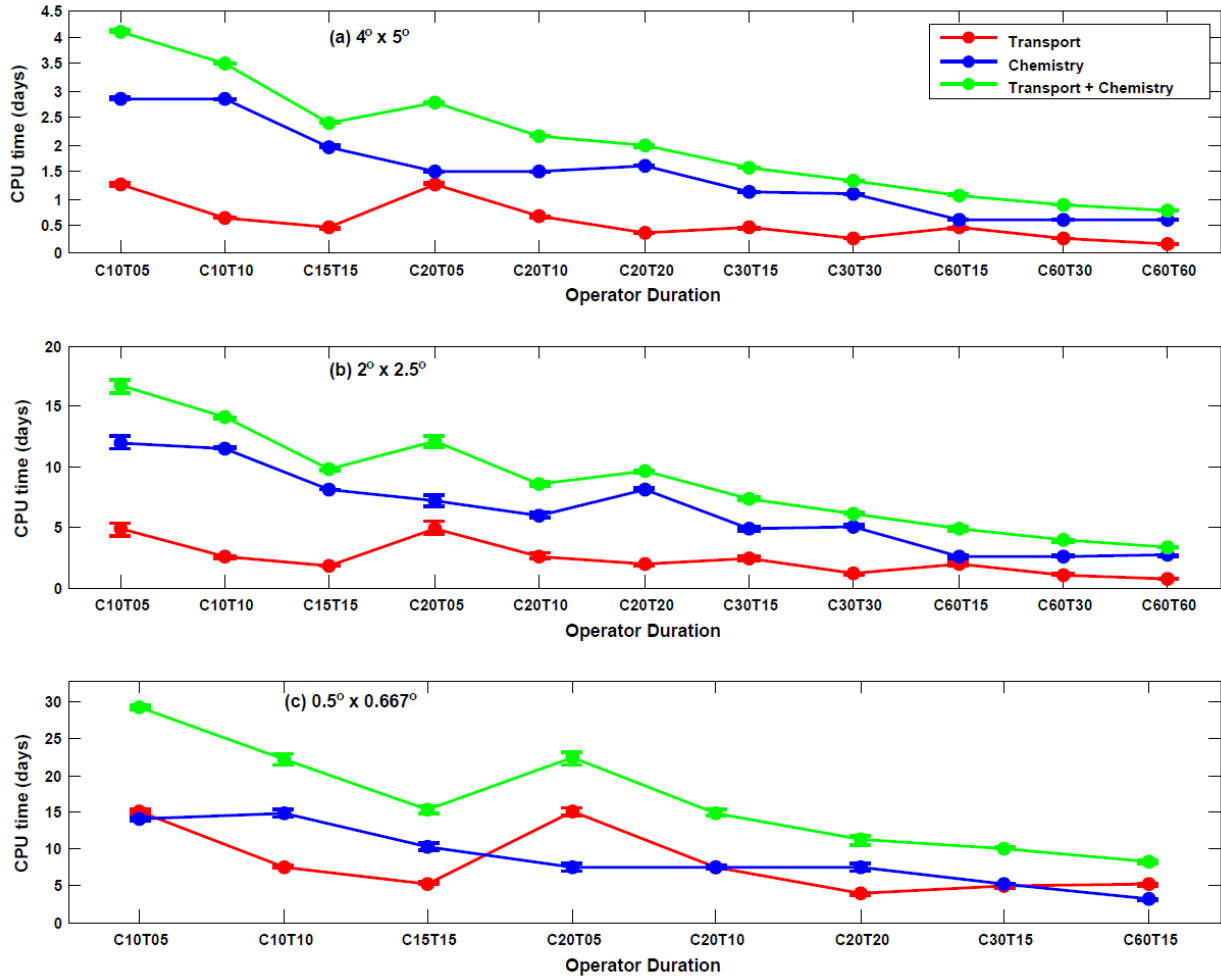
759

760

761

762

763



764

765 Figure 1: CPU time for GEOS-Chem simulations with various operator durations at three
 766 horizontal resolutions. Global simulations are at $4^\circ \times 5^\circ$ (top) and $2^\circ \times 2.5^\circ$ (middle) resolutions.

767 The bottom panel contains results for the average of two nested regions North America and East

768 Asia at $0.5^\circ \times 0.667^\circ$ resolution. Colored lines represent the CPU time for simulating transport (red)

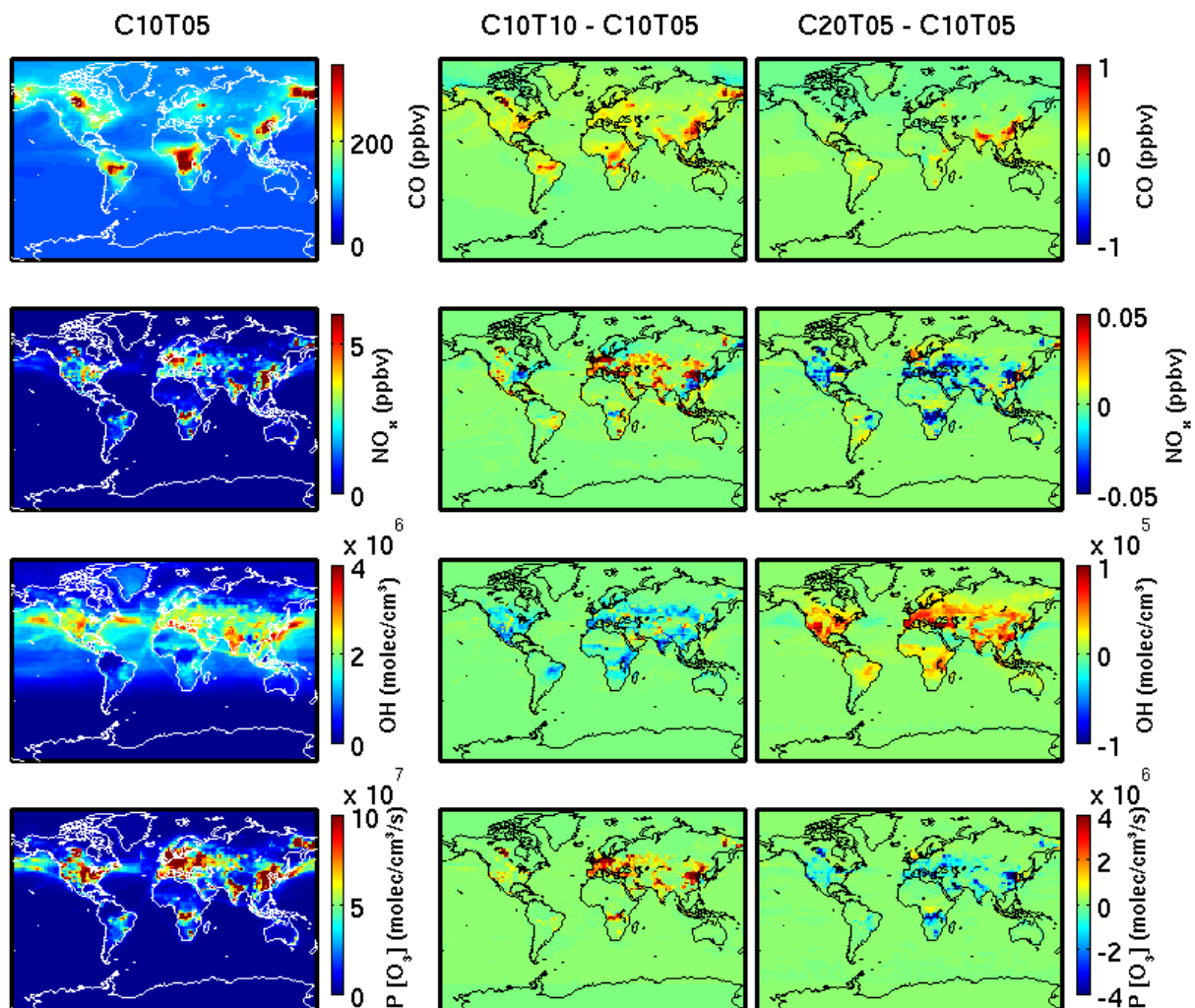
769 and chemical (blue) operators, and the sum of the two (green). Error bars represent standard error

770 over five simulations. Simulations are represented in the abscissa as CccTtt with chemical operator

771 duration, C = cc minutes, and transport operator duration, T = tt minutes.

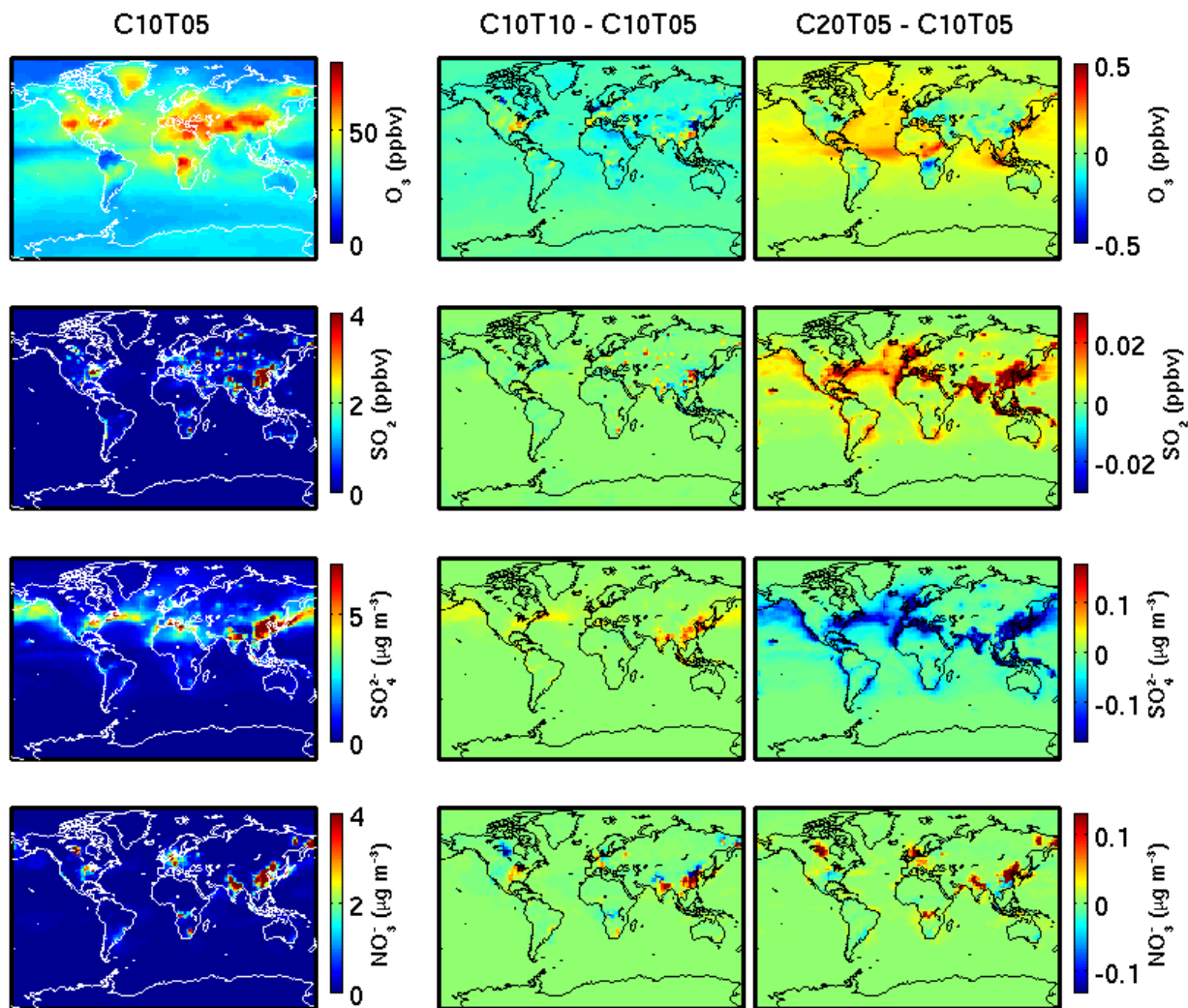
772

773



774
 775 Figure 2a: Sensitivity of simulated species to the duration of chemical and transport operators. The
 776 left column contains monthly mean ground-level concentrations simulated with the shortest
 777 operator duration considered (C10T05) at $2^\circ \times 2.5^\circ$ horizontal resolution. Other columns contain
 778 the absolute differences from doubling the transport operator duration to C10T10 (middle), and
 779 doubling the chemical operator duration to C20T05 (right). Each row from top to bottom
 780 represents carbon monoxide (CO), nitrogen oxides (NO_x), hydroxyl radical (OH), and the
 781 production of ozone ($\text{P}[\text{O}_3]$). Simulations are represented as CccTtt with chemical operator
 782 duration, C = cc minutes, and transport operator duration, T = tt minutes.

783



784

785 Figure 2b: As described in Fig. 2a, but each row from top to bottom represents ozone (O₃), sulfur
 786 dioxide (SO₂), sulfate (SO₄²⁻), and nitrate (NO₃⁻).

787

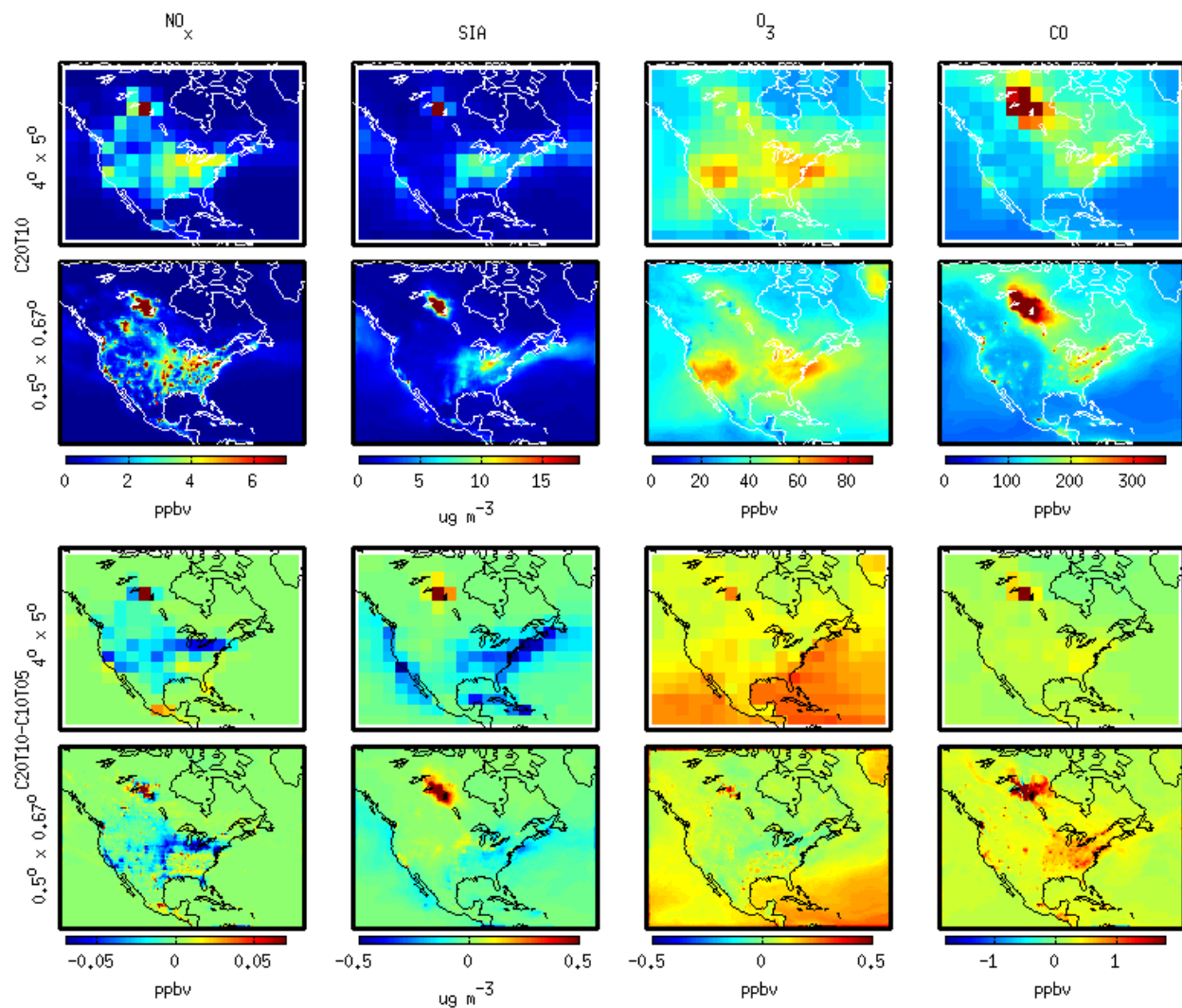
788

789

790

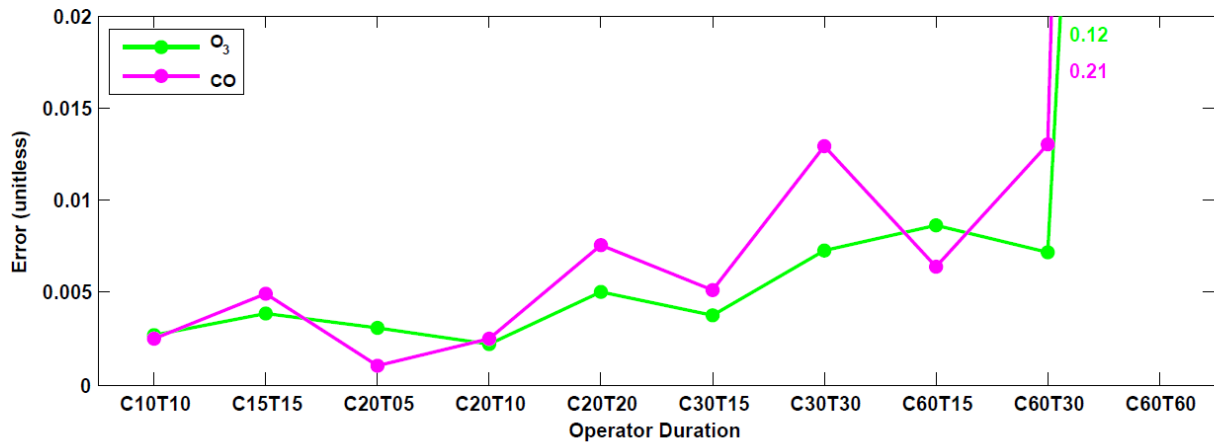
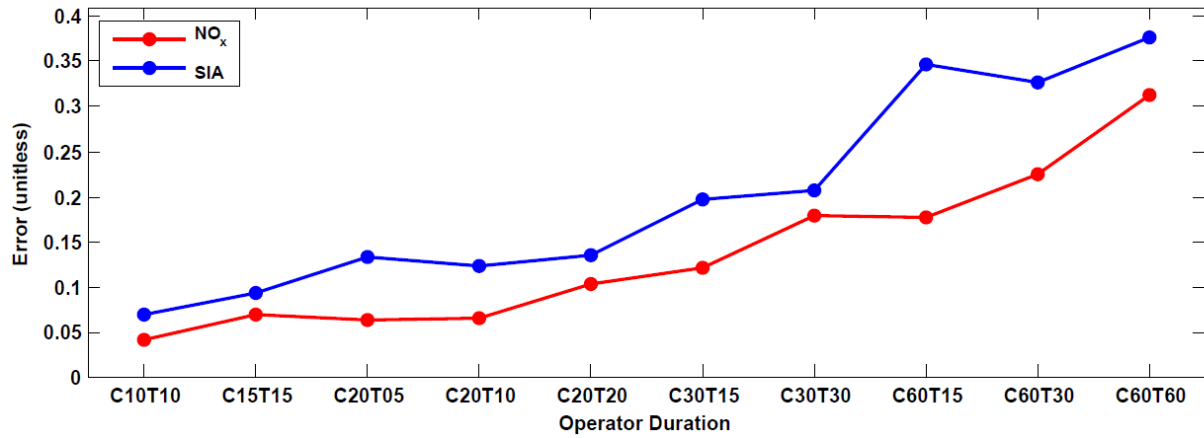
791

792



793
 794 Figure 3: Sensitivity of simulated species to changes in operator duration (C20T10 to C10T05) at
 795 two different horizontal resolutions over North America (global $4^\circ \times 5^\circ$, and nested $0.5^\circ \times 0.67^\circ$
 796 simulations). The upper two rows contain monthly mean ground-level concentrations simulated
 797 with the C20T10 operator duration for $4^\circ \times 5^\circ$ (top row) and $0.5^\circ \times 0.67^\circ$ (second row) resolutions.
 798 The two lower rows contain the monthly mean differences (C20T10 minus C10T05) for $4^\circ \times 5^\circ$
 799 ($4^\circ \times 5^\circ$) (third row) and $0.5^\circ \times 0.67^\circ$ (bottom row) resolutions. Each column from left to right represents
 800 nitrogen oxides (NO_x), secondary inorganic aerosols (SIA), ozone (O_3), and carbon monoxide
 801 (CO).

802



803

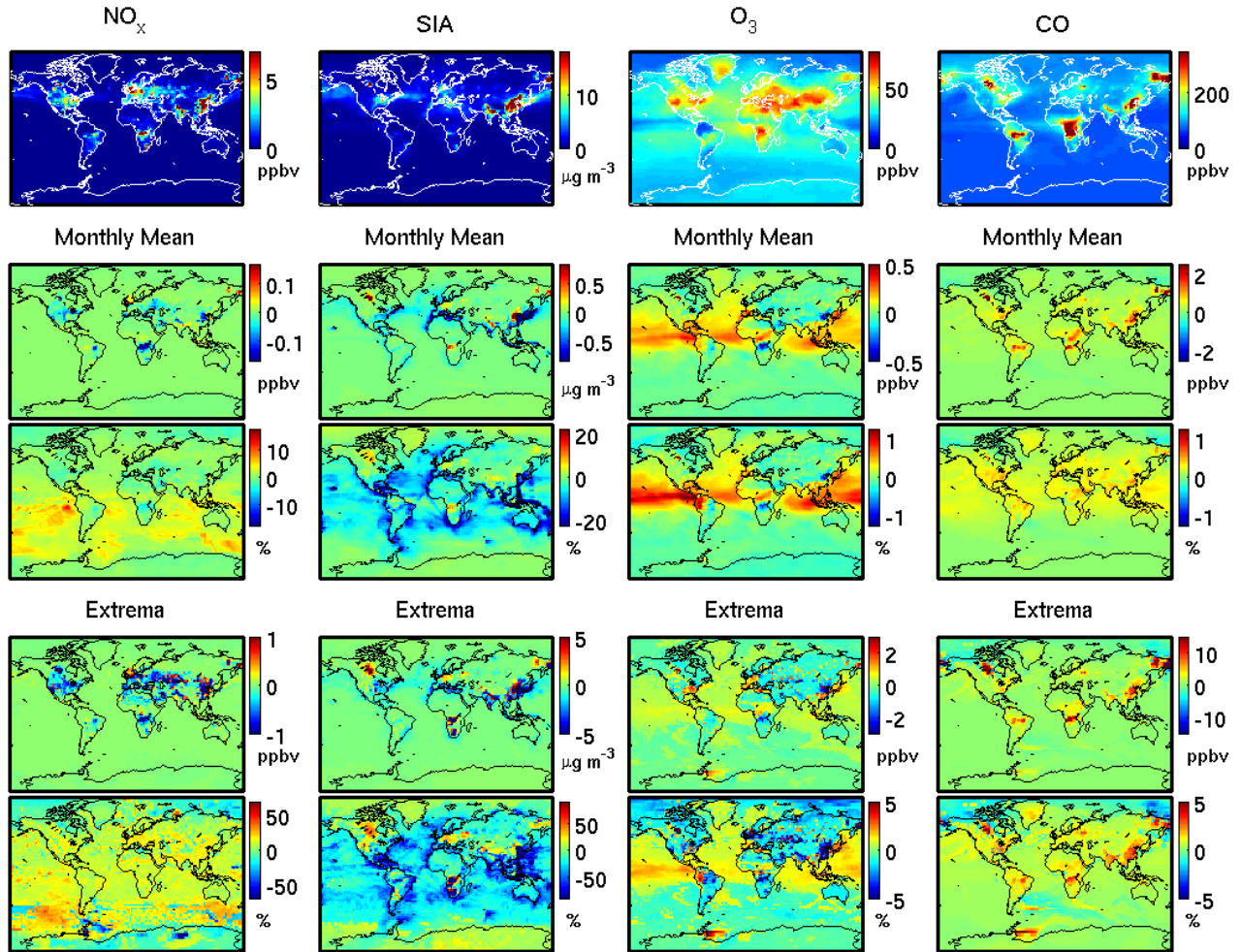
804 Figure 4: Relative simulation error of different species (E_{sim}^s , eq. 3) with various operator durations
 805 at $2^\circ \times 2.5^\circ$ horizontal resolution. Colored lines and dots represent the relative simulation error for
 806 nitrogen oxides (NO_x; red), secondary inorganic aerosols (SIA; blue), ozone (O₃; green), and
 807 carbon monoxide (CO; magenta). Simulations are represented in the abscissa as CccTtt with
 808 chemical operator duration, C = cc minutes, and transport operator duration, T = tt minutes.

809

810

811

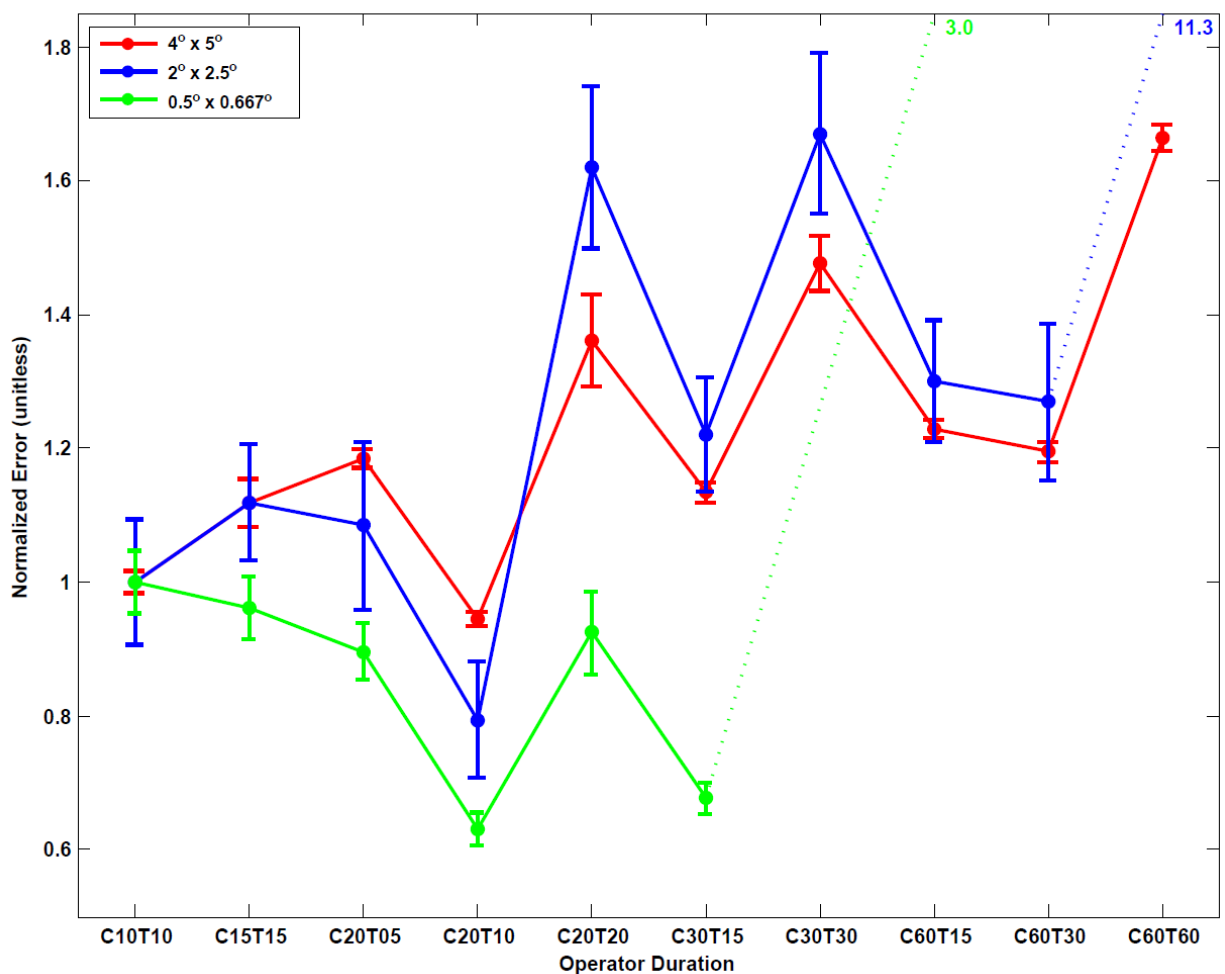
812



813

814

815 Figure 5: Effect on simulated species of changing from the GEOS-Chem traditional operator
 816 durations (C30T15) to the shortest operator durations considered (C10T05). The top row contains
 817 monthly mean ground-level concentrations simulated with the C30T15 operator duration at 2° x
 818 2.5° horizontal resolution. The next two rows contain the monthly mean differences (C30T15
 819 minus C10T05) for absolute (second row) and relative (third row) differences. The two lowest
 820 rows contain the maximum differences (C30T15 minus C10T05) for absolute (fourth row) and
 821 relative (bottom row) differences. Each column from left to right represents nitrogen oxides (NO_x),
 822 secondary inorganic aerosols (SIA), ozone (O₃), and carbon monoxide (CO).



823

824 Figure 6: CPU-time adjusted Composite Normalized Error (CNE, eq. 4) for GEOS-Chem
 825 simulations with various horizontal resolutions and operator durations. Colored lines and dots
 826 represent the CNE for the global simulations at $4^\circ \times 5^\circ$ (red) and $2^\circ \times 2.5^\circ$ (blue), and the nested
 827 simulations at $0.5^\circ \times 0.667^\circ$ (green) horizontal resolutions. Error bars represent standard error in
 828 CPU time. Simulations are represented in the abscissa as CccTtt with chemical operator duration,
 829 C = cc minutes, and transport operator duration, T = tt minutes.